Desalination 548 (2023) 116257

Contents lists available at ScienceDirect

Desalination

journal homepage: www.elsevier.com/locate/desal

Utilization of desalination wastewater for SO_x, NO_x, and CO_2 reduction using NH_3: Novel process designs and economic assessment

Jonghun Lim [a,b,1], Jehun An [a,c,1], Hyungtae Cho [a], Junghwan Kim [a,b,*]

[a] Green Materials and Processes R&D Group, Korea Institute of Industrial Technology, Ulsan 44413, Republic of Korea
[b] Department of Chemical and Biomolecular Engineering, Yonsei University, Seoul 03722, Republic of Korea
[c] Department of Chemistry and Chemical Engineering, Inha University, Incheon 22212, Republic of Korea

HIGHLIGHTS

- Desalination wastewater recovery process is designed for air pollutants reduction.
- Feedstock restriction of pollutant absorbents is possible to be solved.
- Environmental contamination by desalination wastewater is prevented.
- Economic feasibility can increase by CO_2 and SO_x utilization.

GRAPHICAL ABSTRACT

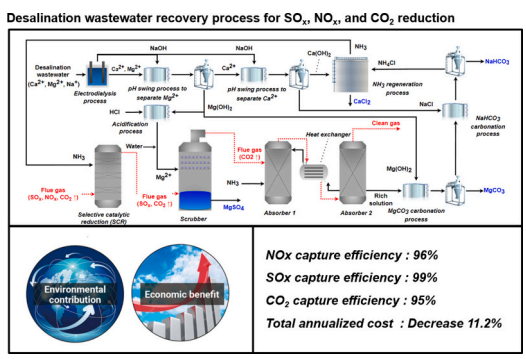

ARTICLE INFO

Keywords:
Desalination
Metal ions
CO_2 capture and utilization
SO_x capture and utilization
NO_x capture

ABSTRACT

Many countries discharge considerable amounts of desalination wastewater directly into the ocean, which cause environmental pollution, destruction of ecosystems, and economic losses. Desalination wastewater contains valuable metal ions such as Na^+, Ca^{2+}, and Mg^{2+}, which react with carbonate and sulfate ions; therefore, it has the high potential to reduce the NO_x, SO_x, and CO_2. Thus, this study designed process for the utilization of desalination wastewater to capture and utilize NO_x, SO_x, and CO_2 using NH_3. A process model was developed, which was composed of following three steps: (1) metal ion separation in desalination wastewater based on pH swing processes for separating Ca^{2+} and Mg^{2+} as $Ca(OH)_2$ and $Mg(OH)_2$, respectively; (2) NO_x capture and SO_x capture and utilization using generated $Mg(OH)_2$, and (3) CO_2 capture and utilization using NH_3. Subsequently, to demonstrate the economic validity of the suggested process, an economic assessment was conducted and total annualized costs (TACs) of the conventional and proposed processes were compared. As a result, ~96 % of NO_x was captured, the SO_x capture efficiency was 99 %, and ~94.7 % of CO_2 was captured. Thus, a reduction of 11.2 % in the TAC was achieved using the proposed process, indicating its high economic feasibility.

* Corresponding author at: Green Materials and Processes R&D Group, Korea Institute of Industrial Technology, Ulsan 44413, Republic of Korea.
E-mail address: kjh31@kitech.re.kr (J. Kim).

[1] Jonghun Lim and Jehun An contributed equally as first authors.

https://doi.org/10.1016/j.desal.2022.116257
Received 19 May 2022; Received in revised form 30 October 2022; Accepted 14 November 2022
Available online 5 December 2022

1. Introduction

Considerable amounts of desalination wastewater are directly discarded in many countries in the process of supplying feasible water [1,2]. The desalination wastewater contains high concentrations of metal ions such as Ca^{2+}, Mg^{2+}, and Na^{+}, and because these useful metal ions react with carbonates and sulfate ions, they can be used for the capture and utilization of SO_x, NO_x, and CO_2 [3,4]. However, most of the desalination wastewater is discarded rather than used, causing serious environmental pollution, such as the destruction of the ecosystem, and economic losses [5]. In recent years, rather than discarding the metal ions in desalination wastewater, efforts have been made to investigate their reuse, and a few previous studies addressed their utilization. Shin et al. proposed a porous polymer to recover the uranyl in seawater [6]. The proposed polymer is capable of removing 90 % of uranyl. Quist-Jensen et al. suggested membrane crystallization to treat the nanofiltration retentate and desalination reject brine [7]. As a result, 99.6 % of K, 100 % of Na and 86.1 % of Ni is recovered from the desalination wastewater. Ali et al. provided a new perspective of isolation of valuable mineral from the produced water [8]. The experiment results shows, 16.4 kg of NaCl per cubic meter of produced water is possible to be recovered. Na et al. proposed the utilization of wastewater as a source of Mg production with CO_2 capture [9]. As a result, 94 % of Mg(OH)2 is possible to be recovered from the desalination wastewater. Among these studies, one investigated the use of desalination wastewater to capture and utilize CO_2 and SO_x to reduce the greenhouse gas emission and air pollution [1]. In their study, NaOH is generated from the desalination wastewater and used for metal ion separation as a buffer solution. Then the Ca^{2+} and Mg^{2+} are separated as a form of $Ca(OH)_2$ and $Mg(OH)_2$, respectively, through metal ion separation based on the difference in the pH level. Subsequently, the generated $Ca(OH)_2$ is used for SO_x capture, thereby producing $CaSO_4$ (i.e. desulfurization gypsum), which is then commercialized. Finally, the CO_2 is captured using the generated NaOH and then carbonated using the formed $Ca(OH)_2$ and $Mg(OH)_2$. As a result of the carbonation, $CaCO_3$ and $MgCO_3$ are also produced, which can be commercialized.

Despite the substantial contribution of the previous study towards the use of desalination wastewater for CO_2 and SO_x utilization, several major limitations persist. These limitations are briefly discussed subsequently. First, the previously mentioned study uses $Ca(OH)_2$ rather than $Mg(OH)_2$ to capture and utilize SO_x. However, $Ca(OH)_2$ generates scales such as $CaSO_4 \bullet 2H_2O$ and $CaSO_3 \bullet 0.5H_2O$ in the scrubber, which causes serious problems and increases the cost of maintenance significantly. In addition, $Ca(OH)_2$ has a relatively higher molar weight compared to $Mg(OH)_2$, and thus, a scrubber with a high capacity scrubber is required, which also increases the total capital cost. Second, using NaOH for CO_2 capture and utilization causes serious corrosion problems in the absorber facility. Because NaOH is strong base, corrosion generally occurs in absorber, which increases maintenance costs and decreases process stability. In addition, the NaOH is impossible to be regenerated and just discharged as a form of the $NaHCO_3$, thus has a problem of the feedstock availability. Finally, previous studies did not consider the NO_x capture (i.e., denitrification) procedure; the NO_x was assumed to be already treated. Conventional denitrification uses NH_3 as an absorbent of the NO_x; the NO_x is converted to N_2, which is not harmful. Using NH_3 increases the operating cost and complicates the utilization process because the NO_x is emitted into the atmosphere as N_2. Thus, the efficient use of NH_3 is important, but it has not been considered in the previous study.

To overcome these limitations, this study proposes a novel process for the utilization of desalination wastewater for SO_x, NO_x, and CO_2 reduction using NH_3, and the economic validity of the proposed process is addressed. The capture and utilization processes of SO_x, NO_x, and CO_2 are integrated using metal ions such as Ca^{2+}, Mg^{2+}, and Na^{+} in desalination wastewater. The aim of this work is to overcome limitations of the previous study by efficiently using desalination wastewater and capturing and utilizing SO_x, NO_x, and CO_2 for environmental protection. The novel contributions of this work are as follows.

1) This study is the first to attempt to enable SO_x, NO_x, and CO_2 capture and utilization at the same time using metal ions in desalination wastewater with NH_3.

2) Because the suggested novel process uses metal ions in desalination wastewater to capture and utilize SO_x, NO_x, and CO_2, it is proper solution for addressing the environmental contamination by desalination wastewater and the feedstock restrictions on conventional absorbents.

3) Because the proposed process uses $Mg(OH)_2$ for SO_x capture and utilization, the problem caused by scales in the scrubber can be prevented. The SO_x is captured by $Mg(OH)_2$ and is converted to $MgSO_3$ and $MgSO_4$, which are soluble in pure water and do not cause scales in the scrubber. In addition, the molar mass of $Mg(OH)_2$ is less than that of $Ca(OH)_2$. Thus, the capacity of the scrubber can be reduced, which indicates decrease in the capital cost.

4) The proposed process uses NH_3 for CO_2 capture and utilization, which prevents corrosion of the absorber. In addition, NH_3 has an advantage of high stability, CO_2 capture efficiency, and low regeneration energy compared to NaOH, which reduces the operating cost. Furthermore, NH_3 is regenerated during the NH_3 reproduction process and is reused during the NO_x capture process. Therefore, the NH_3 is used efficiently.

2. Methodology

2.1. Process overview

Fig. 1 shows an overview of the proposed desalination wastewater recovery process, which is comprised of following three steps: (1) metal ion separation from desalination wastewater, (2) NO_x capture and SO_x capture and utilization, and (3) CO_2 capture and utilization. Next, we presented a brief description of each step.

Step 1. Metal ion separation from desalination wastewater.

First, metal ions, Mg^{2+} and Ca^{2+}, are separated using NaOH, which is generated from the electrodialysis stage of the wastewater desalination process. The NaOH is used as a buffer solution to control the pH level. Mg^{2+} is separated as a form of $Mg(OH)_2$ at a pH of 8.5–11 using the pH swing process for separating Mg^{2+}, and Ca^{2+} is sequentially separated as a form of $Ca(OH)_2$ at a pH of 11–13 using the pH swing process for separating Ca^{2+} [10]. Subsequently, the separated $Mg(OH)_2$ is used for SO_x capture and utilization, and the carbonation of ionic CO_2 and $Ca(OH)_2$ is used to regenerate NH_3 in the NH_3 regeneration process. The residual desalination wastewater in which the Mg^{2+} and Ca^{2+} are removed has high concentration of NaCl and is used for the $NaHCO_3$ carbonation process.

Step 2. NO_x capture and SO_x capture and utilization.

Because the selective catalytic reduction (SCR) requires the high temperature condition of 300 °C or higher, the NO_x is first captured to efficiently use the heat of the high temperature flue gas. In SCR, NO_x is captured using NH_3 and converted to N_2, which is not harmful to the environment. Subsequently, the denitrated flue gas enters the scrubber and SO_x is captured and utilized. To capture and utilize the SO_x, the separated $Mg(OH)_2$ is used as an SO_x absorbent. Because $Mg(OH)_2$ is insoluble in pure water, HCl is added during acidification to ionize the $Mg(OH)_2$ at a pH 5–6. Subsequently, the ionized $Mg(OH)_2$ is mixed with water, and then an alkaline slurry is generated and sprayed at the top of the scrubber. The flue gas that is in contact with the alkaline slurry and SO_x is captured as a result of the vapor-liquid contact [11]. Finally, a $MgSO_4 \bullet 7H_2O$ liquid phase, that is, Epsom salt, is generated at the bottom of the scrubber, and the desulfurized flue gas is emitted to the absorber for CO_2 capture and utilization.

Step 3. CO_2 capture and utilization.

Finally, the CO_2 in denitrated and desulfurized flue gas is captured at the absorber, and to capture the CO_2, NH_3 is used as an absorbent. When

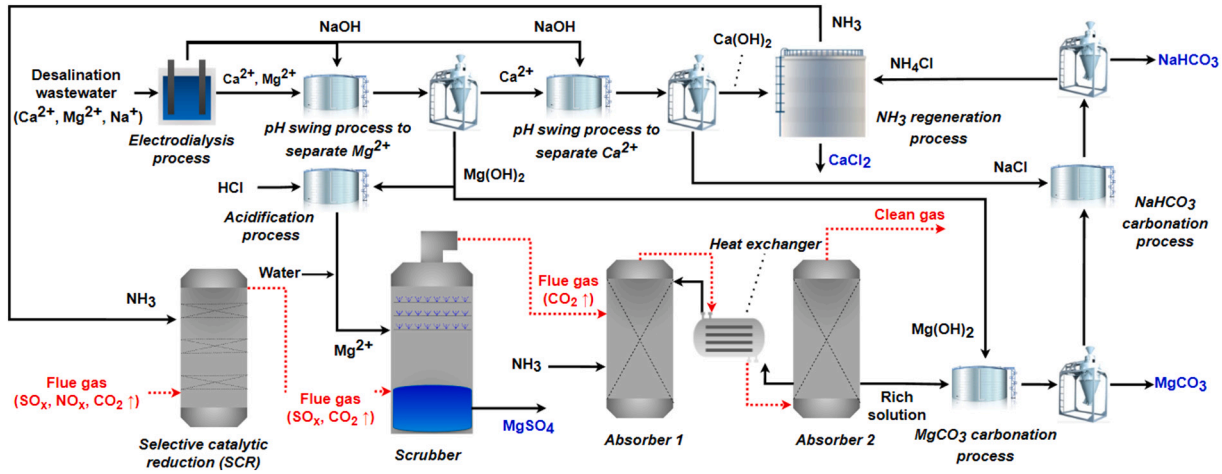

Fig. 1. Overview of the proposed desalination wastewater recovery process.

the CO_2 enters the absorber, it is converted to HCO_3^- and CO_3^- according to the base condition caused by NH_3. Subsequently, the captured CO_2 is carbonated to generate $MgCO_3$ during an $MgCO_3$ carbonation process using the $Mg(OH)_2$, followed by the sequential carbonation of $NaHCO_3$ using the residual desalination wastewater, which has a high NaCl concentration. The remaining NH_4Cl is reacted with $Ca(OH)_2$ during the NH_3 regeneration process, and as a result of the reaction, NH_3, H_2O, and $CaCl_2$ are produced. The generated NH_3 is reused for NO_x capture, and the $CaCl_2$ is commercialized.

2.2. Process model

Fig. 2 shows the process model of the proposed desalination wastewater recovery process. To develop a model this process, Aspen Plus V11.0 from Aspen Tech® was used, and the electrolysis process of the desalination wastewater was modeled using MATLAB® version R2020b from MathWorks.

The proposed process requires a thermodynamic model representing the electrolyte to simulate a reaction involving various ions. Therefore, in this study, the ENRTL-RK model was used, and the correlation between ions in the existing NRTL model was supplemented [12]. The ENRTL–RK model combines ENRTL (Electrolyte nonrandom two liquid) model with the Redlich-Kwong (RK) model [13]. The ENRTL model is applied for the nonideal electrolyte liquid phase, while the RK model is applied to the state equation of the gas phase. The ENRTL model is a widely applied property model for process simulations of electrolyte systems with mixed solvents. The equations for the ENRTL are as follows (Eq. (1)).

$$ln(\gamma^i) = \frac{\sum_{j=1}^{n} x_j \tau_{ji} G_{ji}}{\sum_{k=1}^{n} x_k G_{ki}} + \sum_{j=1}^{n} \frac{x_j G_{ij}}{\sum_{k=1}^{n} x_k G_{kj}} \left(\tau_{ij} - \frac{\sum_{m=1}^{n} x_m \tau_{mj} G_{mj}}{\sum_{k=1}^{n} x_k G_{kj}} \right) \tag{1}$$

where

$$G_{ij} = exp(-\alpha_{ij}\tau_{ij}),$$

$$\alpha_{ij} = \alpha_{ij_0} + \alpha_{ij_1} T,$$

and

$$\tau_{i,j} = A_{ij} + \frac{B_{ij}}{T} + \frac{C_{ij}}{T^2} + D_{ij} ln(T) + E_{ij} T^{F_{ij}}$$

The following equation represents the RK model (Eq. (2)).

$$P = \frac{RT}{V_m - b} - \frac{a}{\sqrt{T} \cdot V_m (V_m + b)} \tag{2}$$

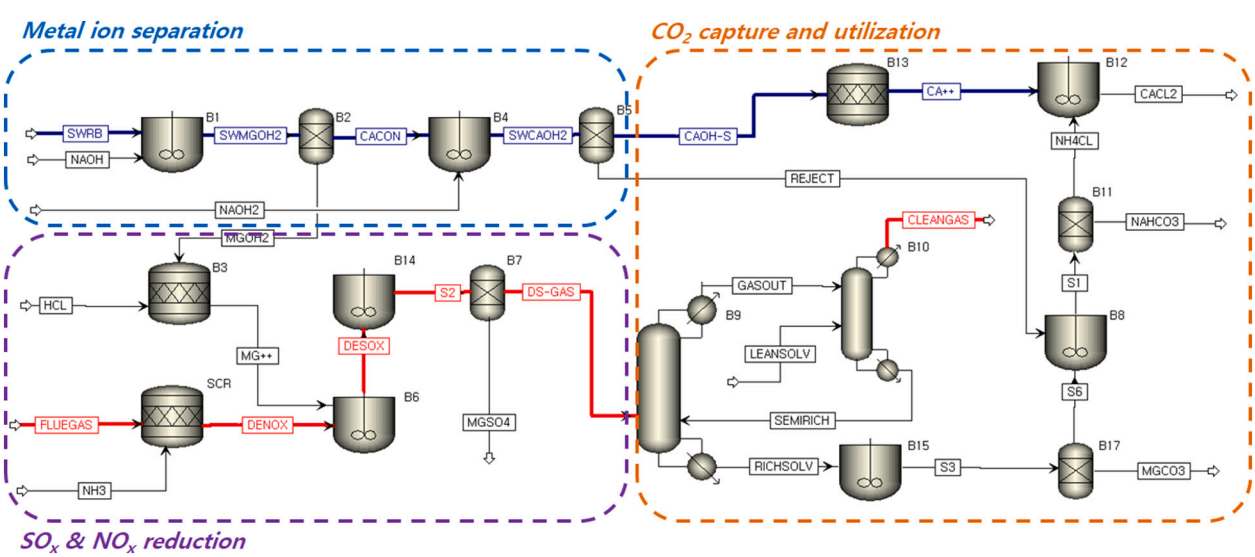

Fig. 2. Process model of the proposed desalination wastewater recovery process.

where,

a : constant for attractive potential of moleculesb

: constant that accounts for volume.

According to the ENRTL-RK model, in an aqueous phase, every stream has no temperature, pressure, or concentration gradient. Streams are mixed ideally and achieve chemical equilibria. These equilibria are automatically predicted in Aspen plus by calculating the electrolyte dissociation and salt precipitation.

2.2.1. Metal ion separation of desalination wastewater

The metal ions, Mg^{2+} and Ca^{2+}, are separated at different pH levels, and NaOH is utilized as a buffer solution for each pH swing process (B1, B4). The NaOH is obtained from the NaCl in desalination wastewater through cholor-alkali electrolysis [14,15], which is modeled using MATLAB® version R2020b. The reaction of the electrolysis of NaCl for NaOH production is as follows (Eqs. (3)–(6)).

$$2Na^+ + 2Cl^- \rightarrow Cl_2 + 2Na^+ + 2e^- \quad (3)$$

$$2Cl^- \rightarrow Cl_2 + 2e^- \quad (4)$$

$$2H_2O + 2e^- \rightarrow H_2 + 2OH^- \quad (5)$$

$$Na^+ + OH^- \rightarrow NaOH \quad (6)$$

In general, the NaOH produced from electrolysis should be limited to low concentrations, due to the instability of the membranes at high pH level and the stable pH range of the electrodialysis process is 10.5 to 11.5 [16]. The pH level of the solution in electrodialysis process in this work is 10.7, and thus it is possible to be stable. Subsequently, the generated NaOH (NAOH, NAOH2) is used to separate Mg^{2+} and Ca^{2+} through a pH swing process as a buffer solution. Subsequently, it is split at the two pH swing processes, that is, process to separate Mg^{2+} (B1) and process to separate Ca^{2+} (B4), and the solubility difference between each metal ion at various pH levels is applied by converting $Mg(OH)_2$ and $Ca(OH)_2$, respectively. First, the Mg^{2+} is separated as a form of $Mg(OH)_2$ at a pH of 8.5–11 in B1 according to the following equation (Eq. (7)).

$$Mg^{2+} + 2OH^- \leftrightarrow Mg(OH)_2 \quad (7)$$

Subsequently, the Ca^{2+} is sequentially separated as a form of $Ca(OH)_2$ at pH 11–13 in B4 according to the following equation (Eq. (8)).

$$Ca^{2+} + 2OH^- \leftrightarrow Ca(OH)_2 \quad (8)$$

Subsequently, the separated $Mg(OH)_2$ is used for SO_x capture and utilization, and the carbonation of the ionic CO_2 and the $Ca(OH)_2$ is used to regenerate NH_3 through an NH_3 regeneration process. The residual desalination wastewater from which the Mg^{2+} and Ca^{2+} are removed has a high NaCl concentration and is used for the $NaHCO_3$ carbonation process. To model B1 and B4, the RCSTR model was used, and the generated $Mg(OH)_2$ (MGOH2) and $Ca(OH)_2$ (CAOH-S) are separated using the Sep model (B2, B5).

2.2.2. NO_x capture and SO_x capture and utilization

To capture the NO_x, this work used the SCR process. The flue gas entered the SCR process, which contained a catalyst, and the NO_x was converted to N_2, which is not harmful to the environment, contrast to adding NH_3 (Eqs. (9)–(11)) [17].

$$4NH_3 + 4NO + O_2 \rightarrow 4N_2 + 6H_2O \quad (9)$$

$$2NH_3 + NO + NO_2 + O_2 \rightarrow 4N_2 + 6H_2O \quad (10)$$

$$8NH_3 + 6NO_2 + O_2 \rightarrow 7N_2 + 12H_2O \quad (11)$$

To improve the NO_x capture efficiency, the selection of a proper catalyst is very important. The NO_x capture efficiency differs according to the operating temperature of the SCR process; thus, the operating temperature of the SCR process should be considered when selecting the catalyst. Recently, catalysts such as titanium oxides, manganese oxides, and tungsten oxide have been employed in many SCR processes; especially nickel based-catalysts, as they have abundant surface acidity sites and high N_2 selectivity [18]. Thus, a nickel-based catalyst was used to capture the NO_x in the proposed process. The NH_3 used in the SCR process was obtained from the NH_3 regeneration process, which generated NH_3 according to the reaction with NH_4Cl and $Ca(OH)_2$. To model the SCR process, the RSTOIC model was used, and the conversion rate of NH_3 was specified as 96 % based on the study by Wang et al. The composition of the flue gas (FLUEGAS) that was added to the SCR process was set to NO (200 ppm), NO_2 (300 ppm), SO_x (700 ppm), CO_2 (15.5%), H_2O (3%), O_2 (16.5%), and N_2 (65%), and the operating temperature was specified as 300 °C [19].

Second, the SO_x in the denitrated flue gas was captured using an alkaline slurry that contained water and $Mg(OH)_2$, which was generated from the pH swing process for separating Mg^{2+} and the acidification process. SO_x causes air pollution, such as haze and acid rain, and reacts with water in air, thereby generating sulfuric acid. Thus, many thermal power plants employ the flue gas desulfurization (FGD) process. In particular, wet flue gas desulfurization (WFGD) is generally employed because of its high desulfurization efficiency [20]. This study uses the separated $Mg(OH)_2$ as an absorbent to capture and utilize the SO_x. Because $Mg(OH)_2$ is insoluble in pure water, HCl is added during acidification to ionize the $Mg(OH)_2$ at a pH of 5–6 (Eq. (12)) [11].

$$Mg(OH)_2 \rightarrow Mg^{2+} + 2OH^- \quad (12)$$

Subsequently, the ionized $Mg(OH)_2$ is mixed with water and alkaline slurry is generated. The alkaline slurry is then sprayed at the top of the scrubber. The flue gas contact with the alkaline slurry and SO_x is captured as a result of the vapor-liquid contact (Eqs. (13)–(15)) [20].

$$SO_2 + H_2O \rightarrow H_2SO_3 \quad (13)$$

$$H_2SO_3 \rightarrow H^+ + HSO_3^- \quad (14)$$

$$HSO^- \rightarrow H^+ + SO_3^{2-} \quad (15)$$

As a result of the SO_x capture, HSO_3^- and SO_3^- are generated, and they react with the Mg^{2+}, thereby generating $Mg(HSO_3)_2$ and $MgSO_3$, which are reaction intermediates. The reaction intermediates are oxidized to $MgSO_4$, which is main product. The overall mechanism of the SO_x capture and utilization is as follows (Eqs. (16)–(20)) [21].

$$SO_2 + Mg(OH)_2 \rightarrow MgSO_3 + H_2O \quad (16)$$

$$SO_2 + MgSO_3 + H_2O \rightarrow Mg(HSO_3)_2 \quad (17)$$

$$Mg(HSO_3)_2 + Mg(OH)_2 + 4H_2O \rightarrow 2MgSO_3 + 3H_2O \quad (18)$$

$$SO_2 + H_2O + \frac{1}{2}O_2 \rightarrow SO_4^{2-} + 2H^+ \quad (19)$$

$$MgSO_3 + \frac{1}{2}O_2 \rightarrow MgSO_4 \quad (20)$$

Finally, in the liquid phase at the bottom of the scrubber, $MgSO_4 \bullet 7H_2O$, that is, Epsom salt, is generated [22], and the desulfurized flue gas is emitted to the absorber for CO_2 capture and utilization. The scrubber is modeled by two steps according to the reaction phases that are at the top and bottom of the scrubber. Each step is modeled using the RCSTR model, and the equilibrium constants of above reaction are obtained based on Gibbs' free energy minimization. The specifications of the WFGD scrubber are based on the study by Salehi et al. [21]. and are presented in Table 1.

Table 1
Specification of the WFGD scrubber that uses $Mg(OH)_2$.

Parameter	Value
Reaction temperature	60 °C
Pressure	1 bar
Valid phase	Liquid-vapor
Equilibrium constants	Based on the Gibbs free energy minimization

2.2.3. CO_2 capture and utilization

In general, CO_2 capture and utilization technologies are classified according to solvent absorption, cryogenic distillation, and membrane separation. Owing to its low cost and the high CO_2 capture efficiency, the absorption process with chemical solvents is generally employed to capture CO_2 [23]. This study used NH_3 as the chemical solvent because of its high capture efficiency, fast reaction rate, low degradation rate, and low regeneration energy [24]. Recently, for absorption processes with chemical solvents, the ammonia-based Solvay process is being investigated for CO_2 capture and utilization. The conventional Solvay process is composed of lime kiln, absorber, and NH_3 regeneration processes. First, for lime kiln, $CaCO_3$ is sintered and converted to CaO. Subsequently, $Ca(OH)_2$ is generated at the lime slaker by mixing with water, and the generated $Ca(OH)_2$ is used for NH_3 regeneration. Second, CO_2 is captured in the absorber and is converted to $NaHCO_3$ and NH_4Cl. Finally, generated NH_4Cl is added to the NH_3 regeneration process, reacts with the $Ca(OH)_2$, and then the NH_3 is recovered. The conventional process consumes a lot of energy to sinter $CaCO_3$ [25]. However, the proposed process does not require a sintering procedure as $Ca(OH)_2$ is obtained from desalination wastewater. The denitrited and desulfurized flue gas that is added to the absorber captures the CO_2 and converts it to HCO_3^- and CO_3^-. The concentrations of the HCO_3^- and CO_3^- are determined according to the pH level of the solution [26], and NH_3 is used as a buffer solution. Without ammonia, the acidic nature of the water solution will hinder the dissociation of CO_2 to HCO_3^- and CO_3^{2-} and hence prevent the precipitation of carbonate [27]. Subsequently, Then the $MgCO_3$ is first separated at filter because if $MgCO_3$ is not separated, the $MgCO_3$ lowers the yield of the $NaHCO_3$ production reaction and requires an additional solid-solid phase separation process. The reaction mechanism of carbon dioxide and magnesium ions in an aqueous ammonia solution is as follows (Eqs. (21)–(25)).

$$NH_3 + H_2O \rightarrow NH_4^+ + OH^- \tag{21}$$

$$OH^- + CO_2 \rightarrow HCO_3^- \tag{22}$$

$$HCO_3^- + OH^- \rightarrow CO_3^- + H_2O \tag{23}$$

$$Mg^{2+} + HCO_3^- \rightarrow MgCO_3 + H^+ \tag{24}$$

$$Mg^{2+} + CO_3^{2-} \rightarrow MgCO_3 \tag{25}$$

Subsequently, the solution from which the $MgCO_3$ was separated is added to the $NaHCO_3$ carbonation process and reacted with NaCl. As a result of reaction, the $NaHCO_3$ is generated, and the reaction is as follows (Eqs. (26)–(28)).

$$NaCl(aq) \rightarrow Na^+ + Cl^- \tag{26}$$

$$Na^+ + HCO^- \rightarrow NaHCO_3(s) \tag{27}$$

$$NH_4^+ + Cl^- \rightarrow NH_4Cl \tag{28}$$

The precipitated $NaHCO_3$ is separated using a filter, and the remaining solution, which has NH_4Cl, is reacted with $Ca(OH)_2$ during the NH_3 regeneration process. The reaction of the NH_4Cl and $Ca(OH)_2$ is as follows (Eq. (29)).

$$2NH_4Cl + Ca(OH)_2 \rightarrow CaCl_2 + 2NH_3 + 2H_2O \tag{29}$$

For the absorber, the ENRTL model was used to calculate the reaction coefficient, reaction enthalpy, and Gibbs free energy of CO_2 in aqueous ammonia. Radfrac model which are modeled rate-based condition was used to simulate the CO_2 capture process. The specification of the rate-based distillation column was based on the study by Qi at el [28]. The specification of the each absorber and inlet stream are listed in Table 2.

3. Result and discussion

In this section, the simulation results of the proposed process are presented and discussed, and to demonstrate the NO_x, SO_x, and CO_2 capture efficiency, 12 conventional cases are set. Then, the NO_x, SO_x, and CO_2 capture efficiencies of the suggested process are compared for each conventional case. Finally, to demonstrate the economic feasibility of the proposed process, the total annualized costs are calculated for an economic assessment. Table 3 shows the conventional cases for NO_x, SO_x, and CO_2 capture processes.

3.1. Simulation result

3.1.1. Metal ion separation results

The Mg^{2+} and Ca^{2+} in desalination wastewater are separated at each pH swing process using NaOH as a buffer solution. Table 4 shows the simulation results for Mg^{2+} separation using the pH swing process for separating Mg^{2+}.

From Table 4, it can be observed that ~0.0448 kmol/h of Mg^{2+} is converted to ~0.04 kmol of $Mg(OH)_2$; thus, the conversion rate of $Mg(OH)_2$ is determined to be 89.2 %. The conversion rate of the $Mg(OH)_2$ is determined according to the amount of NaOH that controls the pH level. Since the Gibbs free energy of formation for $CaCO_3$ and $MgCO_3$ are −1129 kJ/kmol and −1029 kJ/kmol, the Mg^{2+} and Ca^{2+} should be separated [19]. Because when carbonation is performed if the both Ca^{2+} and Mg^{2+} ions are abundant, the nucleation and crystallization of $MgCO_3$ are slower than those of $CaCO_3$, and the production rate of $MgCO_3$ are significantly low. Then, in this study, 0.4 kmol/h of 20 wt% of NaOH was used to maximize the separation efficiency of both metal ions. The simulation results of the Ca^{2+} separation using the pH swing process for separating Ca^{2+} are listed in Table 5.

From Table 5, it can be observed that ~0.0276 mol/h of Ca^{2+} was converted to ~0.0263 mol of $Ca(OH)_2$ according to the NaOH. Thus, the conversion rate of the $Ca(OH)_2$ was determined to be 95.3 %. To separate the Ca^{2+}, an additional 1.25 kmol/h of NaOH was used, and the remaining solution from which Ca^{2+} and Mg^{2+} were separated had a high NaCl concentration. The remaining solution was used in the $NaHCO_3$ carbonation process for CO_2 utilization.

3.1.2. NO_x / SO_x capture and utilization results

First, NO_x is captured using the NH_3 that was regenerated using the NH_3 regeneration process. The flue gas is added to the SCR process, which contains a catalyst, and the NO_x is converted to N_2, which is not as harmful to the environment as adding NH_3. The simulation results of the NO_x capture process are presented in Table 6.

From Table 6, it can be observed that 0.0001 kmol/h of NO and

Table 2
Specification of the each absorber and inlet stream.

Parameter	Value	Parameter	Value
Inlet gas temperature	60 °C	Absorber column type	Rate-based calculation model (Radfrac)
Lean solvent temperature	20 °C	Packing type	25 mm Pall ring
Top pressure	2 bar	Number of stages	20
NH_3 concentration, wt%	4.5 %	Total packing height	6.5 m
Lean solvent flowrate	162 L/h	inner diameter	0.6 m

Table 3
Conventional cases for NOx, SO_x, and CO_2 capture and utilization.

Classification	Case	Process type	Process features
NO_x capture efficiency	N1	*SNCR	No catalyst, NH_3/NO_2 ratio = 1.5
	N2	SNCR	No catalyst, NH_3/NO_2 ratio = 2.0
	N3	**SCR	NiFe-500 catalyst, NH_3/NO_2 ratio = 1.0
	N4	SCR	TiO_2/CeO_2 catalyst, NH_3/NO_2 ratio = 1.0
SO_x capture efficiency	S1	***WFGD	Ca/S ratio = 1.04, pH = 5.9
	S2	WFGD	Ca/S ratio = 1.04, pH = 4.8
	S3	****DFGD	Ca/S ratio = 3
	S4	DFGD	Ca/S ratio = 1.5
CO_2 capture efficiency	C1	*****CCS using NaOH	CO_2 loaded/ NaOH ratio = 0.23
	C2	CCS using NaOH	CO_2 loaded/ NaOH ratio = 0.56
	C3	CCS using MEA	CO_2 loaded/ MEA ratio = 0.18
	C4	CCS using MEA	CO_2 loaded/ MEA ratio = 0.50

*SNCR = Selective non-catalytic reduction, **SCR = Selective catalytic reduction, ***WFGD = Wet flue gas desulfurization, ****DFGD = Dry flue gas desulfurization, *****CCS = Carbon capture and storage.

Table 4
Simulation results of Mg^{2+} separation.

Component	SWRB [kmol/h]	NAOH [kmol/h]	SWMGOH2 [kmol/h]	MGOH2 [kmol/h]	CACON [kmol/h]
H_2O	2.876	0.32	3.196	–	3.1960
Na^+	0.051	0.08	0.131	–	0.1310
OH^-	–	0.08	–	–	–
Ca^{2+}	0.0276	–	0.0276	–	0.0276
Mg^{2+}	0.0448	0	0.0048	–	0.0048
$Mg(OH)_2$	–	–	0.04	0.04	–
$Mg^{2+} \rightarrow Mg(OH)_2$	89.2 %				

Table 5
Simulation results of Ca^{2+} separation.

Component	CACON [kmol/h]	NAOH2 [kmol/h]	SWCAOH2 [kmol/h]	CAOH2 [kmol/h]	REJECT [kmol/h]
H_2O	3.1960	1.000	4.1960	–	4.1960
Na^+	0.1310	0.250	0.3810	–	0.3810
Mg^{2+}	0.0048	–	0.0037	–	0.0037
$Mg(OH)_2$	–	–	0.0011	0.0011	–
OH^-	–	0.250	0.1880	–	0.1880
Ca^{2+}	0.0276	–	0.0023	–	0.0023
$Ca(OH)_2$	–	–	0.0263	0.0263	–
$Ca^{2+} \rightarrow Ca(OH)_2$	95.3 %				

Table 6
Simulation results of NO_x capture process.

Component	FLUEGAS [kmol/h]	NH3 [kmol/h]	DENOX [kmol/h]
NO	0.0001	–	4.8×10^{-6}
NO_2	0.00017	–	6.8×10^{-6}
NH_3	–	0.015355	0.015029
N_2	0.3744	–	0.374692
$NO_x \rightarrow N_2$	96 %		

0.00017 kmol/h of NO_2 react with 0.015355 kmol/h of regenerated NH_3 and are converted to 0.374692 kmol/h of N_2. Thus, the overall NO_x capture efficiency was determined to be 96 %. Generally, NO_x capture processes are classified into selective non-catalyst reduction (SNCR) and selective catalyst reduction (SCR). First, the SCR uses a reducing agent, such as NH_3 or CO, and the flue gas contacts the reducing agent at the column. The fluid enters the catalyst layer, and the NO_x is converted to N_2. The SCR has advantages of a relatively low temperature condition of 300–350 °C and high NO_x capture efficiency. Second, in the SNCR, the NO_x is captured without any catalyst, which requires the high temperature condition of 870–1050 °C, and has a NO_x capture efficiency that is relatively low compared to that of the SCR. Fig. 3 shows the NO_x capture efficiencies of the suggested and conventional processes.

From Fig. 3, the NO_x capture efficiencies of Cases N1 and N2 (SNCR) are approximately 56 % and 59 %, respectively. On the other hand, the NO_x capture efficiencies of Cases N3 and N4 for the SCR are approximately 96 % and 94 %, respectively [18,29]. Finally, because the proposed process uses the SCR process, the NO_x capture is approximately 96 %. The results indicate that the SCR has a higher NO_x capture efficiency compared to that of the SNCR. However, the capital and operating cost of the SCR are significantly higher than those of the SNCR. Therefore, many industries still employ the SNCR due to its economic feasibility. In this study, we use an SCR process with a nickel-based catalyst to maximize the NO_x capture efficiency. However, in practical industrial applications, it is important to select an appropriate process by considering both the economic feasibility and NO_x capture efficiency.

Subsequently, the denitrated flue gas is entered to the scrubber for SO_x capture and utilization. For this process, the $Mg(OH)_2$ that was separated from desalination wastewater using a pH swing process is used as an SO_x absorbent. Because $Mg(OH)_2$ is insoluble in pure water, HCl is added during the acidification process, and the dissolved $Mg(OH)_2$ is sprayed at the top of the scrubber. Through the vapor-liquid contact with the alkaline slurry and flue gas, SO_x is captured, and Table 7 shows the simulation results of the SO_x capture and utilization.

From Table 7, it can be observed that 0.004 kmol/h of SO_x is converted to 0.00039 kmol/h of SO_4^{2-}, and 0.00001 kmol/h of HSO_3^- reacts with 0.04 kmol/h of Mg^{2+}. When the SO_x is captured, HSO_3^- and SO_4^{2-} are generated, and their conversion rates are determined according to the pH level of the liquid phase. As the suggested process uses $Mg(OH)_2$, SO_4^{2-} is abundant because of the high pH level. Although SO_2 is also converted to HSO_3^-, the amount is very small, and $MgSO_3 \bullet 3H_2O$ and $MgSO_3 \bullet 6H_2O$, which are formed by the reaction of Mg^{2+} and HSO_3^- ions, are produced in very small amounts. Most of the converted SO_4^{2-} ions react with Mg^{2+} ions at the bottom of the scrubber to produce Epsom salt, which is widely used in textile, tanning, and agricultural industries. Fig. 4 shows the SO_x capture efficiencies of the proposed and conventional processes.

From Fig. 4, the SO_x capture efficiencies of Cases S1 and S2 (WFGD) are approximately 94 % and 97 %, respectively [30,31]. Furthermore,

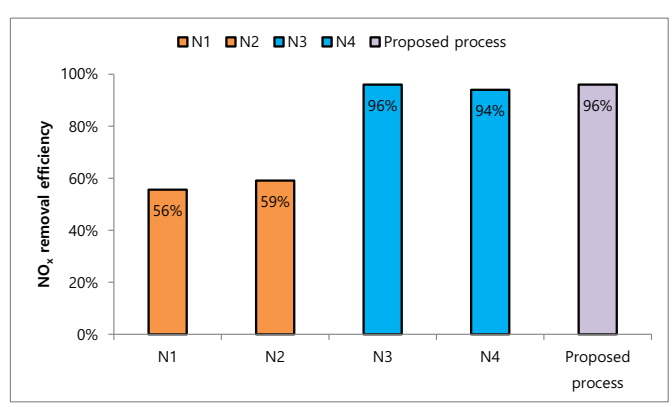

Fig. 3. NO_x capture efficiency of the suggested and conventional processes.

Table 7
Simulation results of the SO_x capture and utilization.

Component	DENOX [kmol/h]	MG++ [kmol/h]	DS-GAS [kmol/h]	MGSO4 [kmol/h]
Mg^{2+}	–	0.04	0.0396	–
SO_2	0.0004	–	–	–
SO_4^{2-}	–	–	0.00039	–
HSO_3^-	–	–	0.00001	–
$MgSO_4*7H_2O$	–	–	–	0.00039
$SO_2 \rightarrow MgSO_4*7H_2O$	99.9 %			

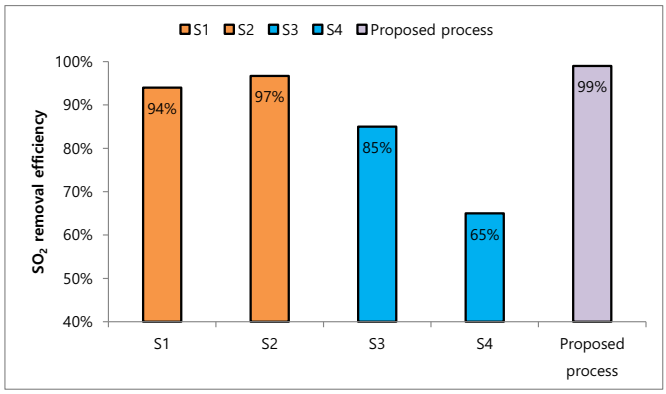

Fig. 4. SOx capture efficiencies of the suggested and conventional processes.

the SO_x capture efficiencies of Cases S3 and S4 (DFGD) are 85 % and 65 %, respectively [32,33]. According to the moisture content of the SO_x absorbent., SO_x capture and utilization processes are generally classified into dry flue gas desulfurization (DFGD) and wet flue gas FGD (WFGD). In both desulfurization processes, a Ca-based SO_x absorbent is generally used, and limestone ($CaCO_3$) and lime (CaO) are representative SO_x absorbents because of their low cost. The results show that the DFGD has an efficiency that is lower compared to that of the WFGD. The reason for this is that the reaction time of the WFGD is longer than that of the DFGD; thus, the removal efficiency of SO_x is high, and the generation of the unreacted absorbent is low. The SO_x capture efficiency of the proposed process is determined to be 99.9 % when $Mg(OH)_2$ is used as an absorbent for SO_x. Because $Mg(OH)_2$ is a relatively strong base compared to $CaCO_3$, it is possible to increase its SO_x capture efficiency.

The conventional SCU uses $CaCO_3$, which is generally obtained in limestone, as the SO_x absorbent. Because other substances, such as SiO_2 and Al_2O_3, decrease the purity of the desulfurization gypsum, which is a by-product of the SCU, the limestone should have a $CaCO_3$ purity of more than 94 wt%, that is, it should be high-grade limestone. However, the reserves of high-grade limestone are only 20 % of the total reserves; thus, the need for a substitute for high-grade limestone is inevitable. In addition, for the SCU that uses $CaCO_3$, CO_2 is inevitably emitted in the removal of SO_x; thus, there is the problem of increased greenhouse gas emission. Lime (CaO) is also employed as an SO_x absorbent and does not emit CO_2; however, it requires the sintering of $CaCO_3$ at high temperatures, which causes additional combustion of fossil fuels and increases costs.

However, in the proposed process, as desalination wastewater is a substitute for high-grade limestone, resource depletion can be avoided. In addition, because the incursion of an expense for providing $CaCO_3$ is not necessary, the cost of mining limestone is reduced, and the generated $MgSO_4 \bullet 7H_2O$ and $MgCO_3$ can be sold, which is cost-effective. In addition, the $Mg(OH)_2$ is used in the SCU system, which is a carbon-neutral desulfurization method. Thus, it is not necessary to consider the additional CO_2 generation.

3.1.3. CO_2 capture and utilization

Finally, the CO_2 in the denitrated and desulfurized flue gas is captured at the absorber, where NH_3 is used as an absorbent. Subsequently, the captured CO_2 exits the ionic-rich flow that contains HCO_3^- and CO_3^{2-}, and the rich flow reacts with Mg^{2+} ions during the $Mg(OH)_2$ carbonation process to generate $MgCO_3$ and NaCl during the $NaHCO_3$ carbonation process to generate $NaHCO_3$. Table 8 shows the simulation results of the CO_2 capture and utilization. From Table 8, it can be observed that 0.1 kmol/h of CO_2 in DS-GAS is added to the absorber and is captured as a form of HCO_3^- and CO_3^{2-}. The conversion rates of HCO_3^- and CO_3^{2-} were calculated to be 82.3 % and 12.4 %, respectively; thus, the CO_2 capture efficiency is determined to be 94.7 %. The captured CO_2 is emitted in the form of CO_3^{2-} and HCO_3^-. Furthermore, the proportion of CO_3^{2-} and HCO_3^- can vary depending on the pH and are mainly in the form of CO_3^{2-} based on the acid-base equilibrium.

Table 9 shows the simulation results of the carbonation process. From Table 9, it can be observed that 0.08231 kmol/h of HCO_3^- is converted to 0.0761 kmol/h of $NaHCO_3$, and 0.01248 kmol/h of CO_3^{2-} is converted to 0.01248 kmol/h of $MgCO_3$. Thus, the conversion rates of the $NaHCO_3$ and $MgCO_3$ are determined to be 92.5 % and 99 %, respectively. The Gibbs free energy of formation of the $NaHCO_3$ and $MgCO_3$ is −852 kJ/mol and −1095 kJ/mol, respectively. Thus, if the $MgCO_3$ is not separated first, the conversion rate of the $NaHCO_3$ is significantly lowered. However, in this study, $MgCO_3$ is separated first; thus, a high conversion rate of $NaHCO_3$ is obtained. Finally, the generated $NaHCO_3$ and $MgCO_3$ are commercialized. Fig. 5 shows the CO_2 capture efficiencies of proposed and conventional processes.

From Fig. 5, it can be seen that the CO_2 capture efficiencies of Cases C1 and C2 (CCS using NaOH) are approximately 90 % and 91 %, respectively [34,35]. Furthermore, the CO_2 capture efficiencies of Cases C3 and C4 (CCS using MEA) are approximately 85 % and 92 %, respectively [36,37]. CO_2 is usually removed from flue gases through chemical absorption using an ethanol amine solution (e.g., MEA or DEA.), ammonia solution, or alkaline solution (e.g., NaOH or KOH) as an absorbent [38]. First, amine has the virtue of high reactivity with CO_2 and low cost, while the amine solution has low CO_2 absorption capacity, and it reacts with other acid components such as formic acid and acetic acid, heat-stable salt is produced, which cause loss of the absorbent during CO_2 capture, resulting in low CO_2 capture efficiency [39]. Second, NaOH is not reusable; thus, there is a problem of an increase in the raw material cost and feedstock availability. In addition, when the CO_2 absorption rate reaches the limited concentration, NaOH emits the CO_2 rather than absorb it. As the CO_2 is captured using NaOH, the NaOH is converted to $NaHCO_3$, and based on the phase equilibrium, the CO_2 is reemitted from the $NaHCO_3$. Thus, there is a limit to the isolation of CO_2 as a metal salt using an NaOH solution [34]. On the other hand, NH_3 has high absorption capacity of CO_2 and fast absorption rate; thus, its CO_2 capture efficiency is high. In addition, NH_3 has high stability of the oxidative and thermal degradation; thus, loss of the solvent can be prevented. Furthermore, in this study, NH_3 is recovered using the $Ca(OH)_2$ that is generated from desalination wastewater, which is an efficient way to use the NH_3. Table 10 shows the simulation results of the

Table 8
Simulation results of the CO_2 capture and utilization.

Component	DS-GAS [kmol/h]	LEANSOLV [kmol/h]	RICHSOLV [kmol/h]	CLEANGAS [kmol/h]
CO_2	0.1	–	–	0.00520
HCO_3^-	5.79×10^{-10}	–	0.08231	–
CO_3^{2-}	3.35×10^{-19}	–	0.01248	–
NH_3	0.0105	0.4294	0.7365	–
OH^-	2.41×10^{-14}	1.03×10^{-8}	3.07×10^{-10}	–
$CO_2 \rightarrow HCO_3^-$	82.3 %			
$CO_2 \rightarrow CO_3^{2-}$	12.4 %			
$CO_2 \rightarrow HCO_3^-$, CO_3^{2-}	94.7 %			

Table 9
Simulation results of carbonation process.

Reaction	In [kmol/h]	Out [kmol/h]	Yield [%]
$HCO_3^- \rightarrow NaHCO_3$	0.08231	0.07610	92.5 %
$CO_3^{2-} \rightarrow MgCO_3$	0.01248	0.01248	99.9 %

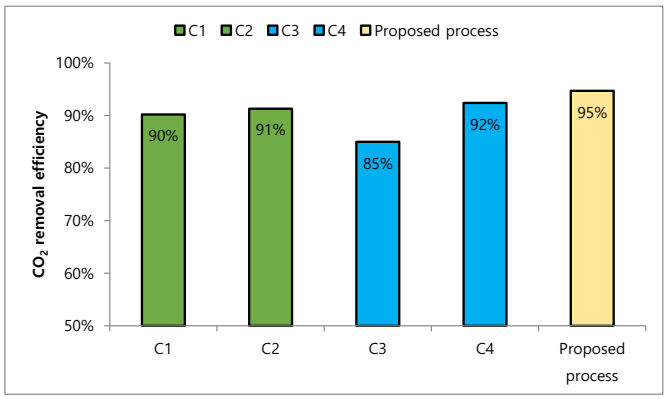

Fig. 5. CO_2 capture efficiencies of proposed and conventional processes.

Table 10
Simulation results of the NH_3 regeneration process.

Component	NH4Cl [kmol/h]	CAOH-S [kmol/h]	CA++ [kmol/h]	CACL2 [kmol/h]
NH_4Cl	0.09676	–	–	0.01456
$Ca(OH)_2$	–	0.0263	0.00004	–
Ca^{2+}	–	–	0.0263	0.0045
NH_3	0.63974	–	–	0.72194
$CaCl_2$	–	–	–	0.02236
$NH_4Cl \rightarrow NH_3$	85.0 %			

NH_3 regeneration process.

From Table 10, it can be observed that approximately 0.09676 kmol/h of NH_4Cl reacts with 0.0263 kmol/h of $Ca(OH)_2$, and as a result of the reaction, 0.0822 kmol/h of NH_3 is regenerated, producing 0.02236 kmol/h of $CaCl_2$. Thus, the regeneration rate of the NH_3 is determined to be 85 %, and the generated $CaCl_2$ can be commercialized for road surfaces, de-icing, freezing-point depression, etc.

3.2. Economic assessment

This section addresses the economic assessment to demonstrate the economic feasibility of the proposed process. To perform the economic assessment, conventional cases are set, which are comprised of the SCR for NO_x capture, WFGD for SO_x capture and utilization, and CCS that uses the MEA for CO_2 capture. The total annualized cost (TAC) of the proposed process and conventional case are calculated. The TAC is determined by adding the equivalent annual cost (EAC) and total product cost (TPC) (Eq. (30)) [40,41].

$$TAC = EAC + TPC \tag{30}$$

3.2.1. Equivalent annual cost

The EAC is the annualized total of capital cost such as equipment cost, land cost, etc. It is determined by dividing the total capital investment (TCI) by the annuity factor (AF) (Eq. (31)) [42].

$$EAC = \frac{TCI}{AF} \tag{31}$$

where, AF is calculated from the discount of the interest rate (r) and number of periods (n):

$$AF = \frac{1 - \frac{1}{(1+r)^n}}{r} \tag{32}$$

r and n are specified as 5 % and 15, respectively.

The TCI is the capital cost, which is composed of land, labor, construction, equipment, etc. It is determined by adding the fixed capital investment (FCI), working capital investment (WCI) and start-up cost (SUC) (Eq. (33)) [43,44].

$$TCI = FCI + SUC + WCI \tag{33}$$

The FCI is the cost of equipment and facilities and is determined from the direct cost (C_{direct}) and indirect cost ($C_{indirect}$) (Eq. (34)) [40,45].

$$FCI = C_{direct} + C_{indirect} \tag{34}$$

C_{direct} is calculated from the inside battery limit cost (C_{ISBL}), which is composed of the cost of equipment, installation, control, pipe and electrical, and outside battery limit cost (C_{OSBL}), which is in turn composed of building, land, and service facilities costs (Eq. (35)) [46].

$$C_{direct} = C_{ISBL} + C_{OSBL} \tag{35}$$

$C_{indirect}$ is cost which is not directly consumed to product, facility, etc. such as security costs, administrative and manpower. The $C_{indirect}$ is determined from the engineering cost ($C_{engineering}$), construction expenses ($C_{construction}$), contractor's fee ($C_{contracotor}$), and contingency cost ($C_{contingency}$) (Eq. (36)) [46].

$$C_{indirect} = C_{engineering} + C_{construction} + C_{contracotor} + C_{contingency} \tag{36}$$

The start-up cost is cost which incurred when starting a facility and it is determined 10 % of the fixed capital investment (Eq. (37)).

$$SUC = 0.1 \times FCI \tag{37}$$

Finally, the working capital investment is capital cost for feedstock, products and spare parts maintenance and it is determined 20 % of the fixed capital investment (Eq. (38))

$$WCI = 0.2 \times FCI \tag{38}$$

Finally, using the above equation, the EAC was calculated, and Table 11 shows the EAC of the conventional and proposed processes.

3.2.2. Total product cost

The TPC is annual cost which incurred during production such as labor cost, raw material cost and utility cost. For TPC calculation, this work set the annual operating to 365 d and the TPC is determined from direct production costs (DPC) and general expenses (GEs) (Eq. (39)).

$$TPC = DPC + GEs \tag{39}$$

The DPC directly affects product production and it can be determined from utility costs, such as raw material costs, water costs, and electricity cost (Eq. (40)).

$$DPC = C_{raw\ materials} + C_{water} + C_{electricity} + C_{maintenance} + C_{labor} + C_{supervision} + C_{operatingsupplies} + C_{laboratory} \tag{40}$$

Table 11
EAC of the conventional and proposed processes [47].

Classification	Percentage of cost	Used	Conventional process [1000 USD/y]	Proposed process [1000 USD/y]
Direct cost				
ISBL				
Equipment cost	100	100	38,533	44,133
Equipment installation	25–55	30	11,560	13,240
Instrumentation and control	8–50	20	7707	8827
Piping	20–80	15	5780	6620
Electrical	15–30	11	4239	4855
OSBL				
Building and building services	10–80	10	3853	4413
Yard improvements	10–20	10	3853	4413
Services facilities	30–80	20	7707	8827
Land	4–8	5	1927	2207
Total direct cost			52,405	60,021
Indirect cost				
Engineering	10	10	3853	4413
Construction expenses	10	10	3853	4413
Contractor's fee	0.5	0.5	193	221
Contingency	5–20	8	3083	3531
Total indirect cost			10,982	12,578
Fixed capital investment	Direct cost + indirect cost		53,753.2	61,565
Startup cost (SUC)	20 % of FCI		10,750.6	12,313
Working capital investment (WCI)	10 % of FCI		5375.32	6157
TCI	SUC + WCI + FCI		69,879.1	80,035
EAC (r = 5 %, n = 15 year)	Eq. (35)		6732.32	7711

where $C_{raw\ materials}$ denotes raw material costs, C_{water} denotes water costs, $C_{electricity}$ denotes electricity costs, $C_{maintenance}$ denotes maintenance costs, C_{labor} denotes labor costs, $C_{supervision}$ denotes supervision costs, $C_{operating\ supplies}$ denotes operating supplies costs, and $C_{laboratory}$denotes laboratory charges.

The GEs is cost which incurred as part of the day-to-day operations and it can be determined by summing the administrative costs ($C_{administrative}$), marketing costs ($C_{marketing}$), and research and development costs ($C_{R\&D}$) (Eq. (41)) [46].

$$GE = C_{admistrative} + C_{marketing} + C_{R\&D} \tag{41}$$

Table 12 shows the TPC of conventional and proposed processes.

3.2.3. Economic assessment results

Table 13 shows the comparison of the EAC, TPC, and TAC of the proposed and conventional processes. It can be observed from the figure that the EAC of the conventional and proposed processes were determined to be 6.73 million USD/y and 7.71 million USD/y, respectively. Because the proposed process required additional equipment for processes such as the pH swing, carbonation, and NH_3 regeneration processes, the EAC of the proposed process was increase by 14.5 % compared to that of the conventional process. Furthermore, the TPCs of the conventional and proposed processes were determined to be 32.08 million USD/y and 26.78 million USD/y, respectively. The TPCs of the proposed process was decreased by approximately 16.5 % because of the decrease in the raw material costs. Despite a slight increase in the electricity cost according to the electrolysis process, the proposed process only requires HCl and makeup NH_3 rather than an expensive absorbent. Finally, the TACs of the conventional and proposed processes were calculated to be 38.81 million USD/y and 34.49 million USD/y, respectively. Thus, the TAC of the proposed process was decreased by 11.2 %, indicating high economic feasibility.

Table 12
Total production costs of the proposed and conventional processes [47].

Classification	Range	Used	Conventional process [1000 USD/y]	Proposed process [1000 USD/y]
Direct production cost				
Local taxes, Insurance	1.5–5 % of FCI	3	1613	1847
Maintenance (M)	1.0–10 % of FCI	4	2150	2463
Operating labor (OL)	15 % of TPC	15	4811	4017
Supervision and support labor (S)	30 % of OL	30	1443	1205
Operating supplies	15 % of M	15	215	246
Laboratory charges	10–20 % of OL	10	481	402
Plant overhead cost OVHD	50–70 % of M + OL + S	60	5043	4611
Electricity	–	Calculated	6696	1279
Raw material	–	Calculated	6656	8232
General expenses				
Administrative cost	15–20 % of OL	15	722	603
Distribution and marketing	2–20 % of TPC	2	642	536
R&D cost	2–15 % of TPC	5	1604	1339
Total production cost	Direct production cost + general expenses		32,076	26,778

Table 13
Comparison of the EAC, TPC and TAC of the proposed and conventional process.

Classification	Conventional process [million USD/y]	Proposed process [million USD/y]
EAC	6.73	7.71
TPC	32.08	26.78
TAC	38.81	34.49

4. Applicability of the proposed process

This section addressed the applicability of the proposed process in actual desalination plants. To address the applicability of the proposed process, the main outcomes of conventional and proposed process is compared. Table 14 shows comparison of the main outcomes of conventional model in the literature with proposed model.

Table 14
Comparison of the main outcomes of conventional model in the literature with proposed model.

Classification	Conventional model [1]	Proposed model
NO_x capture efficiency	0 %	96 %
SO_x capture efficiency	99 %	99 %
CO_2 capture efficiency	91 %	94.7 %
Products	$CaCO_3$, $MgCO_3$, $CaSO_4$	$MgCO_3$, $NaHCO_3$, $CaCl_2$, $MgSO_4$

From the table, although NO_x capture was not considered in the conventional model, the proposed process can capture NO_x using NH_3 and shows a reduction efficiency of 96 %. The use of NH_3 increase the operating cost and since the NO_x is emitted in to the atmosphere as N2 and thus the utilization of NO_x is complicate. However, the proposed model can recover the NH_3 at NH_3 regeneration process, the efficient use of NH_3 is possible. Then, the 99 % of SO_x is capture at conventional and proposed model. The conventional model use the $Ca(OH)_2$ for SOx capture, however the it cause the scales such as $CaSO_4 \bullet 2H_2O$ and $CaSO_3 \bullet 0.5H_2O$ in the scrubber, which causes serious problems and increases the cost of maintenance significantly. In addition, molar weight of $Ca(OH)_2$ is higher than $Mg(OH)_2$, and thus the high capacity scrubber is required. On the other hands, since the proposed process use $Mg(OH)_2$ and thus the problem of the scales and capacity increase can solved. Finally, the CO_2 capture efficiency of the conventional and proposed model is determined by 91 % and 94.7 % respectively. In conventional model, the NaOH is used for CO_2 capture however, when the CO_2 absorption rate reaches the limited concentration, NaOH emits the CO_2 rather than absorb it. As the CO_2 is captured using NaOH, the NaOH is converted to $NaHCO_3$, and based on the phase equilibrium, the CO_2 is reemitted from the $NaHCO_3$. However, the NH3 has high absorption capacity of CO_2 and fast absorption rate; thus, its CO_2 capture efficiency is high. The proposed process shows higher air pollutant reduction efficiency than the conventional process, and also can produce various products such as $MgCO_3$, $NaHCO_3$, $CaCl_2$ and $MgSO_4$. In addition, desalination wastewater is recycled to reduce air pollutants, and the efficiency of the process can be maximized by reusing NH_3 that conventionally cannot be recovered. Therefore, we believe that the proposed process will not only overcome the limitations of the conventional process, but also have a high potential for application to actual desalination plants.

5. Conclusion

In this work, we designed a novel process for the utilization of desalination wastewater for NO_x, SO_x, and CO_2 capture and utilization using NH_3. This study makes two major contributions to the existing literature. First, because the suggested process use the metal ions in desalination wastewater for NO_x, SO_x, and CO_2 capture and utilization, it is an proper solution for the environmental contamination by desalination wastewater and the feedstock restrictions on conventional absorbents. Second, this study proposes an environmental and economical approach for NO_x, SO_x, and CO_2 utilization in the flue gas using only metal ions in desalination wastewater; thus, the approach is efficient and environmentally friendly. The findings of the study are as follows. Approximately 96 % of NO_x was captured, the SO_x capture efficiency was 99 %, and approximately 94.7 % CO_2 was captured. Furthermore, the TACs of the conventional and proposed processes were determined to be 38.81 million USD/y and 34.49 million USD/y, respectively. Thus, the proposed process has a 11.2 % reduction in the TAC, indicating high economic feasibility. Thus, we believe that this study provides valuable insights into the efficient use of desalination wastewater and the capture and utilization of NO_x, SO_x, and CO_2 in a cost-effective and environmentally friendly manner. The Ca and Mg-based products cause fouling of the industrial equipment and thus some mitigation techniques are proposed. Thus, focus on the mitigation techniques should be taken into consideration for rigorous economic assessment in the further studies. In addition, when the actual process is operated, the results may be slightly different from the theoretical simulation results. Therefore, it is necessary to fit detailed parameters and operating conditions.

CRediT authorship contribution statement

Jonghun Lim: Conceptualization, Investigation, Methodology, Formal analysis, Writing – original draft. **Jehun An:** Validation, Writing – original draft. **Hyungtae Cho:** Funding acquisition, Writing – review & editing. **Junghwan Kim:** Supervision, Validation, Funding acquisition, Writing – review & editing.

Declaration of competing interest

The authors declare that they have no known competing financial interests or personal relationships that could have appeared to influence the work reported in this paper.

Data availability

No data was used for the research described in the article.

Acknowledgments

This work was supported by the Korean Institute of Industrial Technology within the framework of the following project: "Development and application of carbon-neutral engineering platform based on carbon emission database and prediction model [grant number KM-22-0348]".

Appendix A. Supplementary data

Supplementary data to this article can be found online at https://doi.org/10.1016/j.desal.2022.116257.

References

[1] S. Cho, J. Lim, H. Cho, Y. Yoo, D. Kang, J. Kim, Novel process design of desalination wastewater recovery for CO2 and SOX utilization, Chem. Eng. J. (2021), 133602, https://doi.org/10.1016/j.cej.2021.133602.
[2] K. Elsaid, M. Kamil, E.T. Sayed, M.A. Abdelkareem, T. Wilberforce, A. Olabi, Environmental impact of desalination technologies: a review, Sci. Total Environ. 748 (2020), 141528, https://doi.org/10.1016/j.scitotenv.2020.141528.
[3] K. Madwar, H. Tarazi, Desalination techniques for industrial wastewater reuse, Desalination 152 (2003) 325–332, https://doi.org/10.1016/S0011-9164(02)01080-9.
[4] E.T. Sayed, N. Shehata, M.A. Abdelkareem, M.A. Atieh, Recent progress in environmentally friendly bio-electrochemical devices for simultaneous water desalination and wastewater treatment, Sci. Total Environ. 748 (2020), 141046, https://doi.org/10.1016/j.scitotenv.2020.141046.
[5] J.S. Chang, Understanding the role of ecological indicator use in assessing the effects of desalination plants, Desalination 365 (2015) 416–433, https://doi.org/10.1016/j.desal.2015.03.013.
[6] Y.H. Sihn, J. Byun, H.A. Patel, W. Lee, C.T. Yavuz, Rapid extraction of uranium ions from seawater using novel porous polymeric adsorbents, RSC Adv. 6 (2016) 45968–45976, https://doi.org/10.1039/c6ra06807c.
[7] C.A. Quist-Jensen, F. Macedonio, E. Drioli, Integrated membrane desalination systems with membrane crystallization units for resource recovery: a new approach for mining from the sea, Crystals 6 (2016), https://doi.org/10.3390/cryst6040036.
[8] A. Ali, C.A. Quist-Jensen, F. Macedonio, E. Drioli, Application of membrane crystallization for minerals' recovery from produced water, Membranes (Basel) 5 (2015) 772–792, https://doi.org/10.3390/membranes5040772.
[9] C.-K. Na, H. Park, E.H. Jho, Utilization of waste bittern from saltern as a source for magnesium and an absorbent for carbon dioxide capture, Environ. Sci. Pollut. Res. 24 (2017) 1–10, https://doi.org/10.1007/s11356-017-9913-5.
[10] J. Johnston, The solubility-product constant of calcium and magnesium carbonates, J. Am. Chem. Soc. 37 (1915) 2001–2020, https://doi.org/10.1021/ja02174a006.
[11] H. Lee, S. Jin, B. Choi, I. Kim, in: Design and Operation of 3MW Pilot Plant of Mg (OH) ₂ Flue Gas Desulfurization Process, 2001, pp. 0–4.
[12] B.J. Sherman, Thermodynamic and Mass Transfer Modeling of Aqueous Hindered Amines for Carbon Dioxide Capture, 2016.
[13] J. Lim, J. Kim, Optimization of a wet flue gas desulfurization system considering low-grade limestone and waste oyster Shell, J. Korea Soc. Waste Manag. 37 (2020) 263–274, https://doi.org/10.9786/kswm.2020.37.4.263.
[14] F. Du, D.M. Warsinger, T.I. Urmi, G.P. Thiel, A. Kumar, J.H. Lienhard, Sodium hydroxide production from seawater desalination brine: process design and energy efficiency, Environ. Sci. Technol. 52 (2018) 5949–5958, https://doi.org/10.1021/acs.est.8b01195.
[15] T. Budiarto, E. Esche, J.-U. Repke, Chlor-Alkali Process Modelowanie I Sterowanie Procesem, Tech. Trans, 2016.
[16] K.-H. Yeon, J.-H. Song, B.-S. Shim, S.-H. Moon, Production of sulfuric acid and ammonia water from ammonium sulfate using electrodialysis with bipolar membrane and ammonia stripping, Korean Membr. J. 7 (2005) 28–33.

[17] S.H. Park, K.-Y. Lee, S.J. Cho, Catalytic technology for NOx abatement using ammonia, Clean Technol. 22 (2016) 211–224, https://doi.org/10.7464/ksct.2016.22.4.211.
[18] R. Wang, X. Wu, C. Zou, X. Li, Y. Du, Nox removal by selective catalytic reduction with ammonia over a hydrotalcite-derived NiFe mixed oxide, Catalysts 8 (2018), https://doi.org/10.3390/catal8090384.
[19] S. Cho, J. Lim, H. Cho, Y. Yoo, D. Kang, J. Kim, Novel process design of desalination wastewater recovery for CO2 and SOX utilization, Chem. Eng. J. 433 (2022), 133602.
[20] P. Córdoba, Status of flue gas desulphurisation (FGD) systems from coal-fired power plants: overview of the physic-chemical control processes of wet limestone FGDs, Fuel 144 (2015) 274–286, https://doi.org/10.1016/j.fuel.2014.12.065.
[21] E. Salehi, B. Eidi, Z. Soleimani, An integrated process consisting of Mg(OH)2 –impregnated ceramic foam filters as adsorbent and Mg(OH)2 as scrubbing solution for intensified desulfurization of flue gas, Sep. Purif. Technol. 216 (2019) 34–42, https://doi.org/10.1016/j.seppur.2019.01.072.
[22] L. Okhrimenko, L. Favergeon, K. Johannes, F. Kuznik, M. Pijolat, Thermodynamic study of MgSO4 – H2O system dehydration at low pressure in view of heat storage, Thermochim. Acta 656 (2017) 135–143, https://doi.org/10.1016/j.tca.2017.08.015.
[23] M.V. Mercedes, Developments and innovation in carbon dioxide (Co2) capture and storage technology, Dev. Innov. Carbon Dioxide Capture Storage Technol. (2010) 1–538, https://doi.org/10.1533/9781845699574.
[24] K. Jiang, H. Yu, L. Chen, M. Fang, M. Azzi, A. Cottrell, K. Li, An advanced, ammonia-based combined NOx/SOx/CO2 emission control process towards a low-cost, clean coal technology, Appl. Energy 260 (2020), 114316, https://doi.org/10.1016/j.apenergy.2019.114316.
[25] H. Lu, E.P. Reddy, P. Smirniotis, Calcium oxide based sorbents for adsorption of CO2 at high temperatures, AIChE Annu. Meet. Conf. Proc. 2005 (2005) 3944–3949.
[26] P. Bumroongsakulsawat, G.H. Kelsall, Effect of solution pH on CO: formate formation rates during electrochemical reduction of aqueous CO2 at sn cathodes, Electrochim. Acta 141 (2014) 216–225, https://doi.org/10.1016/j.electacta.2014.07.057.
[27] M.H. El-Naas, A.F. Mohammad, M.I. Suleiman, M. Al Musharfy, A.H. Al-Marzouqi, A new process for the capture of CO2 and reduction of water salinity, Desalination 411 (2017) 69–75, https://doi.org/10.1016/j.desal.2017.02.005.
[28] G. Qi, S. Wang, H. Yu, P. Feron, C. Chen, Rate-based modeling of CO2 absorption in aqueous NH3 in a packed column, Energy Procedia 37 (2013) 1968–1976, https://doi.org/10.1016/j.egypro.2013.06.077.
[29] L. Zhang, L. Li, Y. Cao, X. Yao, C. Ge, F. Gao, Y. Deng, C. Tang, L. Dong, Getting insight into the influence of SO2 on TiO2/CeO2 for the selective catalytic reduction of NO by NH3, Appl. Catal. B Environ. 165 (2015) 589–598, https://doi.org/10.1016/j.apcatb.2014.10.029.
[30] L. Zhang, Q. Zhang, Y. Cheng, Z. Dong, Field tests and optimal operation research of WFGD for a 600MW power plant, IOP Conf. Ser. Mater. Sci. Eng. 452 (2018), https://doi.org/10.1088/1757-899X/452/3/032099.
[31] F.J. Gutiérrez Ortiz, F. Vidal, P. Ollero, L. Salvador, V. Cortés, A. Giménez, Pilot-plant technical assessment of wet flue gas desulfurization using limestone, Ind. Eng. Chem. Res. 45 (2006) 1466–1477, https://doi.org/10.1021/ie051316o.
[32] B. Hou, H. Qi, C. You, X. Xu, Dry desulfurization in a circulating fluidized bed (CFB) with chain reactions at moderate temperatures, Energy Fuels 19 (2005) 73–78, https://doi.org/10.1021/ef0499751.
[33] F. Scala, M. D'Ascenzo, A. Lancia, Modeling flue gas desulfurization by spray-dry absorption, Sep. Purif. Technol. 34 (2004) 143–153, https://doi.org/10.1016/S1383-5866(03)00188-6.
[34] Y. Guo, Z. Niu, W. Lin, Comparison of removal efficiencies of carbon dioxide between aqueous ammonia and NaOH solution in a fine spray column, Energy Procedia 4 (2011) 512–518, https://doi.org/10.1016/j.egypro.2011.01.082.
[35] W.Y. Choi, C. Aravena, J. Park, D. Kang, Y. Yoo, Performance prediction and evaluation of CO2 utilization with conjoined electrolysis and carbonation using desalinated rejected seawater brine, Desalination 509 (2021), 115068, https://doi.org/10.1016/j.desal.2021.115068.
[36] L.E. Øi, Comparison of aspen HYSYS and aspen plus simulation of CO2 absorption into MEA from atmospheric gas, Energy Procedia 23 (2012) 360–369, https://doi.org/10.1016/j.egypro.2012.06.036.
[37] J.T. Yeh, H.W. Pennline, K.P. Resnik, Study of CO2 absorption and desorption in a packed column, Energy Fuels 15 (2001) 274–278, https://doi.org/10.1021/ef0002389.
[38] D. Cui, S. Yan, X. Guo, F. Chu, Advance in post-combustion CO2 capture with alkaline solution: a brief review, Energy Procedia 14 (2012) 1967–1972, https://doi.org/10.1016/j.egypro.2011.12.1126.
[39] L.S. Tan, A.M. Shariff, K.K. Lau, M.A. Bustam, Factors affecting CO 2 absorption efficiency in packed column: a review, J. Ind. Eng. Chem. 18 (2012) 1874–1883, https://doi.org/10.1016/j.jiec.2012.05.013.
[40] J. Lim, H. Cho, J. Kim, Optimization of wet flue gas desulfurization system using recycled waste oyster shell as high-grade limestone substitutes, J. Clean. Prod. 318 (2021), 128492, https://doi.org/10.1016/j.jclepro.2021.128492.
[41] J. Lim, S. Jeong, J. Kim, Deep neural network-based optimal selection and blending ratio of waste seashells as an alternative to high-grade limestone depletion for SOX capture and utilization, Chem. Eng. J. (2021), 133244, https://doi.org/10.1016/j.cej.2021.133244.
[42] J. Lim, J. Lee, H. Cho, J. Kim, Model development of amine regeneration process with electrodialysis reclamation unit, Comput. Aided Chem. Eng. 50 (2021), https://doi.org/10.3390/min7110207.
[43] Y. Kim, J. Lim, H. Cho, J. Kim, Novel mechanical vapor recompression-assisted evaporation process for improving energy efficiency in pulp and paper industry, Int. J. Energy Res. (2021) 1–19, https://doi.org/10.1002/er.7390.
[44] Y. Kim, J. Lim, J.Y. Shim, S. Hong, H. Lee, H. Cho, Optimization of Heat Exchanger Network via Pinch Analysis in Heat Pump-Assisted Textile Industry Wastewater Heat Recovery System, 2022.
[45] J. Lim, J. Lee, I. Moon, H. Cho, J. Kim, Techno-economic comparison of amine regeneration process with heat-stable amine salt reclaiming units, Energy Sci. Eng. (2021) 1–15, https://doi.org/10.1002/ese3.1000.
[46] Y.S. Jeong, J. Jung, U. Lee, C. Yang, C. Han, Techno-economic analysis of mechanical vapor recompression for process integration of post-combustion CO2 capture with downstream compression, Chem. Eng. Res. Des. 104 (2015) 247–255, https://doi.org/10.1016/j.cherd.2015.08.016.
[47] M.R.M. Abu-Zahra, J.P.M. Niederer, P.H.M. Feron, G.F. Versteeg, CO2 capture from power plants. Part II. A parametric study of the economical performance based on mono-ethanolamine, Int. J. Greenhouse Gas Control 1 (2007) 135–142, https://doi.org/10.1016/S1750-5836(07)00032-1.